Synthesis, Characterization, and Catalytic Performance of Highly Dispersed Co-SBA-15

Chuan Wang, Sangyun Lim, Guoan Du, Codruta Zoican Loebicki, Nan Li, Salim Derrouiche, and Gary L. Haller*

Department of Chemical Engineering, Yale University, P.O. Box 208286, New Haven, Connecticut 06520-8286

Received: February 27, 2009; Revised Manuscript Received: June 19, 2009

Highly dispersed cobalt on SBA-15 was successfully prepared by a post synthesis grafting of cobalt. Of the cobalt precursors tested, Co(II) acetylacetonate was found to be the best source for high dispersion of cobalt. The Co-SBA-15 catalysts were characterized with different techniques: N_2 physisorption, XRD, TPR, TEM, and X-ray adsorption analysis. The mesoporous structure of SBA-15 was retained after cobalt grafting with up to 10 wt % Co loading. There were no large cobalt oxide particles formed, which indicates all the cobalt ions are highly dispersed on the surface and the direct bonding to the silica surfaces results in a high reduction temperature (1123 K) relative to Co oxides. X-ray absorption analysis demonstrates a local structure of Co ions with all Co ions isolated and bonded with oxygen. XANES analysis requires that the local environment for Co ions be that of either a distorted tetrahedral or an octahedral structure and the fitting of EXAFS data further shows a Co−O bond coordination number of 3.58 ± 0.48, confirming that the Co is in a distorted tetrahedral environment. The catalytic activity of Co-SBA-15 catalyst was studied for the synthesis of carbon single walled nanotubes (SWNT). The high reduction stability of Co-SBA-15 is presumed to make a favorable catalyst for this high temperature reaction. Raman spectroscopy and TEM photographs show that good quality carbon SWNT was synthesized by Co-SBA-15. Moreover, Co-SBA-15 has a higher yield of carbon SWNT compared with Co-MCM-41 (C16 alkyl template) under the same reaction conditions.

1. Introduction

Cobalt-incorporated (during synthesis) mesoporous catalyst Co-MCM-41 was recently demonstrated to be a good catalyst for the synthesis of carbon single-walled nanotubes (SWNT).[1–4] It is believed that the growth mechanism of carbon SWNT on Co-MCM-41 catalyst involves reduced cobalt metal particles acting as the catalytic sites for both dissociation of CO and aggregation of carbon atoms to form the carbon SWNT.[5] The most important step is to control the particle size of the reduced cobalt because carbon SWNT can only grow from small cobalt particles[6] and the diameter of the SWNT is primarily controlled by the cobalt particle size.[7–10] A narrow diameter distribution is desired, and this requires small and stable cobalt particles of uniform size. In Co-MCM-41, cobalt ions (as Co^{2+}) are substituted for silicon in the MCM-41 silica framework, which results in a high dispersion of cobalt ions. It has been demonstrated by X-ray absorption analysis that essentially all cobalt ions are isolated in the MCM-41 silica matrix. Analysis of EXAFS data shows that cobalt ions are bonded directly with only oxygen atoms (which in turn, are bonded to silicon cations) in a distorted tetrahedral surrounding and there is no measurable Co−Co bonding. The high dispersion of cobalt ions with high stability is correlated with a high reduction temperature. The maximum reduction temperature of Co-MCM-41 (made from C16 alkyl template) is about 1033 K. Such high reduction stability also makes Co-MCM-41 a preferred catalyst for the synthesis of carbon SWNT by CO disproportionation, which is a high-temperature reaction (973−1023 K). In early work, the yield of carbon SWNT was only about 3 wt % using 3 wt % Co-MCM-41 (C16 alkyl template).[11] A route to increase the yield of carbon SWNT is to increase cobalt loading. However, there is a limit of cobalt loading in Co-MCM-41 because the mesoporous structure starts to collapse when the cobalt loading exceeds 4 wt %.[12] This is partly due to the thin wall of the MCM-41 structure. Thus, we wish to find another support which gives not only high dispersion and high reduction stability of cobalt ions, but also has a high cobalt loading. That is, small Co metal particles are desired for SWNT synthesis, and these are difficult to stabilize against sintering at the high temperatures required for CO disproportionation to SWNT. One mechanism of stabilization against sintering is anchoring Co metal particles to Co cations in a silica matrix,[13] so that anchoring potential is increased when Co cations have a high reduction stability.

SBA-15 is a mesoporous material similar to MCM-41 but has larger pores and thicker walls.[14] The synthesis conditions used to prepare SBA-15 are different from MCM-41. SBA-15 materials are synthesized using a triblock polymer as a structure-directing agent and tetraethylorthosilicate as a silica source under acid conditions[14,15] while MCM-41 materials are synthesized under extremely basic conditions by a sol−gel method. The different synthesis conditions make it difficult to synthesize Co-SBA-15 in the same way as Co-MCM-41. Co-MCM-41 was synthesized by simply adding cobalt precursors during the synthesis of siliceous MCM-41. However, this method does not work for Co-SBA-15 because there is very limited solubility of Co salts in the solution required to dissolve the polymer, e.g., pH < 2. Essentially all cobalt ions remain unreacted in the liquid phase after the synthesis. Increasing the pH of the synthesis solution is not an option because the mesoporous structure of SBA-15 cannot be maintained at pH values higher than 2. An alternate method to introduce cobalt into SBA-15 support is required.

One of the most commonly used methods for making metal oxide catalyst is impregnation. Cobalt contained SBA-15 catalysts have been synthesized by the impregnation method

* To whom correspondence should be addressed: E-mail: gary.haller@yale.edu. Phone: 1-203-432-4378. Fax: 1-203-432-4387.

10.1021/jp901823v CCC: $40.75
Published on Web 07/23/2009

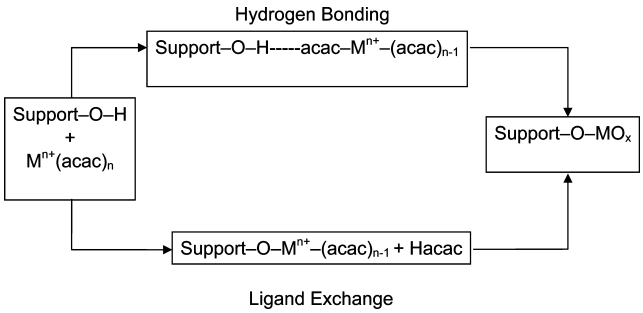

Figure 1. Schematic of the grafting mechanism of metal acetylacetonate on the support.[19]

with different cobalt precursors.[16,17] However, impregnated Co-SBA-15 showed low dispersion of cobalt ions and low reduction stability. The reduction temperature of impregnated cobalt Co-SBA-15 is around 723 K, which is the reduction temperature of surface cobalt oxide. Such impregnated Co-SBA-15 is not useful in the synthesis of carbon SWNT because all the cobalt ions will be reduced and aggregated into large particles (tens of nanometers) at high reaction temperature.

Another approach for the creation of supported metal oxide catalysts, recognized as molecular designed dispersion (MDD) or atomic layer deposition (ALD), which consists of the adsorption and subsequent thermolysis of supported metal acetylacetonate ($M^{n+}(acac)_n$) complexes (or similar precursors) has been studied in the last two decades.[18–27] We call it a grafting method here because a metal precursor is grafted on the surface of the support and will be incorporated into the surface after calcination. Such a MDD or ALD method for the synthesis of supported metal oxide catalysts consists of two steps: (i) irreversible adsorption of the complex by hydrogen bonding or by a ligand exchange mechanism and (ii) decomposition of the grafted complex in an oxygen-containing atmosphere at elevated temperatures. The process of this grafting method is visualized in Figure 1. There are two possible pathways for the adsorption of the complexes: (i) through hydrogen bonding between an acetylacetonate ligand and the surface hydroxyls or (ii) by ligand exchange in which a covalent metal−oxygen support bond is formed while an acetylacetonate ligand (Hacac) is lost. Van Der Voort has proved the first pathway—hydrogen bonding for the adsorption of $VO(acac)_2$ on silica.[21] He defined an R value as the ratio of adsorbed acac ligands to the adsorbed vanadium species. If the adsorption mechanism is hydrogen bonding, the R value should be 2. Otherwise, R is 1 for the ligand exchange pathway. Their experimental results showed that R was 2, which proved the hydrogen bonding mechanism. Some other work also confirmed this mechanism for the adsorption of metal acetylacetonate.[22,28]

Recently, Iglesia and co-workers used a similar grafting method for the synthesis of highly dispersed tungsten oxide catalyst on mesoporous silica.[29] They used organic solvents and anhydrous conditions to control the deposition of tungsten oxide species onto the silica surface. In our work, Co-SBA-15 was synthesized by a two-step method combining the synthesis of siliceous SBA-15 and then deposition of cobalt ions onto SBA-15 using the grafting method with different Co complexes. The synthesized Co-SBA-15 was characterized by different techniques to demonstrate the high dispersion of cobalt ions and high reduction stability, e.g., XRD, N_2 physisorption, TEM, and TPR. X-ray absorption experiments were conducted to help understand the local environment of cobalt ions in the synthesized Co-SBA-15 catalyst and the reduction to metal. The catalytic efficiency of Co-SBA-15 was tested with our desired reaction, carbon SWNT synthesis. Raman spectra and TEM photographs showed the production of good quality carbon SWNT. Also, because higher cobalt loading was attained, a higher yield of carbon SWNT was achieved compared with the original Co-MCM-41 catalyst under the same reaction conditions.[1–4]

2. Experimental Section

2.1. Preparation of Catalysts. The cobalt-grafted SBA-15 catalysts were synthesized following a two-step method. First, mesoporous siliceous SBA-15 was synthesized according to a procedure described by Stucky and co-workers using a triblock copolymer ($EO_{20}PO_{70}EO_{20}$, P123, Aldrich) as the structure directing agent and tetraethylorthosilicate (TEOS, Aldrich, 98%) as the silica source under acidic conditions.[14,15] Four grams of the $EO_{20}PO_{70}EO_{20}$ was dissolved in 30 g of H_2O and 120 g of 2 M HCl. The mixture was continually stirred until the copolymer was completely dissolved. Then 8.5 g of tetraethylorthosilicate (TEOS) was slowly added dropwise. The mixture was stirred for an additional 10 min and then transferred to polypropylene bottles. The bottles were held at 313 K for 20 h. Afterward, the samples were aged at 373 K in the autoclave for 48 h. After cooling, the solids were washed and filtered with deionized water, and then allowed to air-dry. The as-synthesized samples were heated in helium from room temperature to 813 K at 0.5 K/min, then stabilized in helium for another hour; after that, the carrier gas was switched from helium to air for 5 h to remove the organic residues at 813 K. The mass ratio of each component during synthesis was $EO_{20}PO_{70}EO_{20}$/HCl/TEOS/H_2O = 2:4.38:4.25:70.62.

The cobalt-grafted SBA-15 catalysts were synthesized following a controlled grafting process through atomic layer deposition (ALD). Different cobalt precursors—Co(II) chloride, Co(III) acetylacetonate, and Co(II) acetylacetonate—were tested. Only the samples grafted using Co(II) acetylacetonate showed a high dispersion and high reduction stability. Cobalt-grafted SBA-15 catalysts discussed in this paper refer to those grafted by Co(II) acetylacetonate, unless a different cobalt precursor is indicated. The cobalt precursor solution was prepared by dissolving cobalt in 150 mL of anhydrous toluene (Aldrich, 99%) for 3 h. The solution was refluxed at 383 K for 3 h with N_2 flowing through the apparatus to completely dissolve the cobalt compound resulting in a 6.3×10^{-3}, 1.4×10^{-2}, 2.4×10^{-2}, and 3.8×10^{-2} M solution for grafting that would result in a maximum loading of 10, 20, 30, and 40 wt %. The as-calcined SBA-15 was simultaneously suspended in 80 mL of anhydrous toluene and refluxed in flowing N_2 to remove any adsorbed water. The cobalt precursor solution was then added into the SBA-15/toluene suspension, and the mixture was refluxed for another 3 h. Nitrogen gas was flowed to remove any physisorbed water and to prevent contact with water in air. Thus, the flowing of nitrogen gas was continued throughout the reaction. The reaction mixture was cooled, filtered, and washed with toluene to ensure that there was no unreacted cobalt precursor left on the SBA-15. The solids were then dried overnight in ambient air. The calcination procedure for the as-synthesized Co-SBA-15 was the same as for the siliceous SBA-15.

2.2. Characterization Techniques. Nitrogen physisorption isotherms at 77 K were measured with a Quantachrome Autosorb-3b static volumetric instrument. Prior to measurement, the samples were outgassed at 473 K to a residual pressure below 10^{-4} torr. A Baratron pressure transducer (0.001−10 Torr) was used for low-pressure measurements. The specific surface

area was calculated following the method of Brunauer, Emmet, and Teller (BET).[30] The pore size and pore size distribution were calculated by the Barrett, Joyner, Halenda (BJH) method[31] using the desorption branch of the isotherm.

X-ray diffraction (XRD) measurements were conducted using a Bruker AXS D8Focu diffractometer (Cu Kα, $\lambda = 0.15$, 4 nm, 40 KV, 30 mA).

Hydrogen temperature-programmed reduction (TPR) measurements were conducted using a gas chromatograph (Agilent 6890 plus) with a thermal conductivity detector (TCD). Prior to each TPR run, the sample cell was purged with He at room temperature, then the temperature was increased to 1123 K at 5 K/min, and held for 1 h at 1123 K. The reduction gas flowing though the cell was 5 vol % H_2 in argon. A frozen acetone trap was installed between the sample cell and the gas chromatograph to condense the water produced from the reduction.

Transmission electron microscopy (TEM) images were taken by a Tecnai 12 microscope from FEI Co.

The final loading of cobalt was measured by inductivity coupled plasma (ICP) methods at Galbraith Lab., Inc.

X-ray absorption analysis was performed at beamline X23 A2, National Synchrotron Light Source, Brookhaven National Laboratory. The data were collected at the cobalt K edge (7709 eV). EXAFS in the transmission mode was recorded from 200 eV below to 900 eV above the cobalt K edge. The spectra collected were analyzed using the UWXAFS analysis package.[32] The theoretical EXAFS functions for cobalt species generated by the FEFF6 program were used to fit the experimental data in order to calculate the Co−O shell coordination numbers.[33] The hydrated samples were prepared by exposing the Co-SBA-15 catalysts in ambient conditions. The dehydrated samples were prepared by in situ heating the sample wafer in ultra high purity helium at 573 K for 30 min.

2.3. Catalytic Performance. The catalytic activity of Co-SBA-15 was measured by our desired experiment, synthesis of carbon SWNT. The catalyst was first prereduced at high temperature (873 or 973 K) in pure H_2 for 30 min, and then purged with He for another 30 min to remove any H_2 (∼20 times the volume of the reactor). The reaction temperature was held at 1073 K using pure CO as the reactant. After reaction, the color of the catalyst changed from blue to black, the color of carbon SWNT. Raman spectroscopy and TEM characterizations proved the existence of high quality SWNT. The approximate yield of carbon SWNT based on the total weight of catalyst was about 6% for the 6 wt % Co-SBA-15 by TGA.

3. Results and Discussion

3.1. Characterization of Catalysts. The goal of this work was to find a novel cobalt catalyst, which not only shows high dispersion and high reduction/thermal stability for Co^{2+} ions/cobalt metal particles similar to Co-MCM-41 but also has a high cobalt loading. Different characterization techniques were used including XRD, X-ray absorption, N_2 physisorption, TEM, and TPR. XRD, N_2 physisorption, and TEM were used to identify the physical properties of the catalyst, such as surface area, pore size, pore size distribution, Co^{2+} ion environment and reduction, and cobalt particle size. Temperature programmed reduction was used to study the reduction behavior of Co-SBA-15, which is a very important property in the catalytic synthesis of carbon SWNT. Quantitative TPR was also used to calibrate the actual cobalt loading by comparing the TPR peak area of each sample with the standard sample which was analyzed by ICP by Galbraith.

3.1.1. X-ray Diffraction (XRD). Figures 2 and 3 depict the low and high range of 2θ XRD graphs for Co-SBA-15 synthesized by two different cobalt precursors, $CoCl_2$ and Co(II) acetylacetonate. Typically, the low-range diffraction pattern shows evidence of highly ordered hexagonal mesoporous structure with three deflections at 2θ value between 0.5° and 3°, corresponding to the (100), (110), and (200) peaks (Figures 2a and 3a). Due to the detection limit of the equipment, the strongest (100) peak was partially overwhelmed by the background signal below 1°. Both graphs show the same distinct (100), (110), and (200) peaks in the low-range XRD patterns, which illustrates that the ordered hexagonal porous framework is retained after grafting cobalt cations onto siliceous SBA-15. The high-range XRD patterns as shown in Figures 2b and 3b differ greatly. The Co-SBA-15 synthesized from $CoCl_2$ (Figure 2b) shows various scattering and diffraction peaks. This indicated that instead of covalently bonding onto the surface of the SBA-15, cobalt ions merely aggregated on the surface. The crystal structure (after calcinations) can be identified as Co_3O_4 particles from the 2θ values of the diffraction peaks. With an increase of cobalt loading in the initial synthesis solution, more

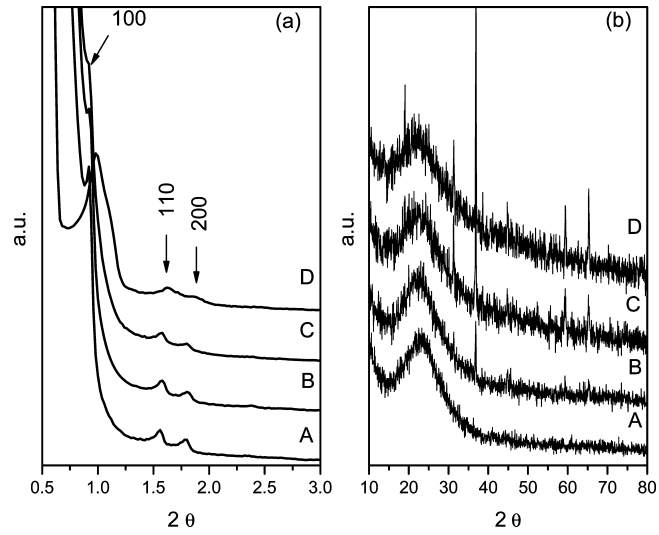

Figure 2. XRD patterns of cobalt-grafted SBA-15 synthesized from $CoCl_2$ at (a) low- and (b) high-range diffraction angles. (A) Pure siliceous SBA-15, (B) 1 wt % Co-SBA-15, (C) 5 wt % Co-SBA-15 with, (D) 10 wt % Co-SBA-15.

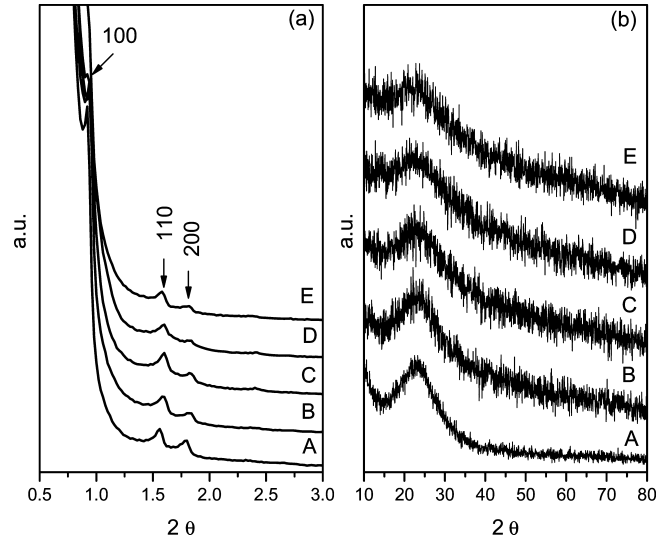

Figure 3. XRD patterns of cobalt-grafted SBA-15 synthesized from Co(II) acetylacetonate at (a) low- and (b) high-range diffraction angle. (A) Pure siliceous SBA-15, (B) 5.7 wt % Co-SBA-15, (C) 8.0 wt % Co-SBA-15, (D) 9.8 wt % Co-SBA-15, (E) 10.4 wt % Co-SBA-15.

TABLE 1: Physical Properties of Si-SBA-15 and Co-SBA-15 Synthesized from $Co(C_5H_7O_2)_2$ with Different Cobalt Loadings

sample ID	actual Co loading (wt %)	BET surface area (m^2/g)	pore diameter (nm)	mesopore volume (cc/g)	total pore volume (cc/g)	mesopore volume/total pore volume
Si-SBA-15	N/A	922	7.0	1.25	1.31	0.95
Si-SBA-15r[a]	N/A	667	6.7	1.0	1.1	0.95
SiSBA-15rc[b]	N/A	650	6.7	1.0	1.09	0.95
Co-SBA-15, 10 wt %[c]	5.7	590	6.7	1.0	1.06	0.94
Co-SBA-15, 20 wt %[c]	8.0	610	6.7	1.03	1.1	0.94
Co-SBA-15, 30 wt %[c]	9.8	595	6.7	1.03	1.08	0.95
Co-SBA-15, 40 wt %[c]	10.4	560	6.7	0.92	0.98	0.94

[a] Si-SBA-15 after refluxing. [b] Si-SBA-15 after refluxing and recalcination. [c] wt % shown in the sample ID is the maximum assuming complete reaction of Co in the synthesis solution.

and larger crystals were formed corresponding to the stronger diffraction signals in Figure 1b. The formation of larger crystals was also confirmed by TEM, which will be discussed later. Figure 3b shows the high-range XRD patterns of Co-SBA-15 synthesized with cobalt(II) acetylacetonate. In contrast with Figure 2b, it did not have any diffraction peaks even with the increase of the initial cobalt up to the equivalent to 40 wt % loading in the synthesis solution. This could either indicate that the cobalt was evenly dispersed within the catalyst or that no cobalt ions are grafted. However, TPR and chemical analysis both showed evidence of significant amounts of cobalt (ranging from 5.7 to 10.4 wt %, see Table 1), an indication that all the cobalt ions are well dispersed in the Co-SBA-15 samples which were grafted with Co(II) acetylacetonate.

3.1.2. N_2 Physisorption. From the XRD analysis, it has been proven that the hexagonal mesoporous structure was retained after cobalt was grafted and by using Co(II) acetylacetonate as a cobalt source, highly dispersed Co-SBA-15 was achieved. XRD analysis only provides information on the local properties of the catalyst. Another primary technique used to measure the average physical properties is N_2 physisorption. Figure 4a and c show the N_2 adsorption/desorption isotherm of calcined siliceous SBA-15 and cobalt-grafted SBA-15 (made from Co(II) acetylacetonate) with different cobalt loadings. The isotherm of calcined siliceous SBA-15 presented a sharp inflection at a relative pressure in the range of 0.65−0.8, an indication of the good quality SBA-15 materials with an uniform mesoporous structure. After cobalt was grafted, the shape of the isotherms of Co-SBA-15 with different cobalt loading was almost identical to the original siliceous SBA-15, having a sharp capillary condensation step in the range of 0.65−0.8. The similar isotherm shapes between Co-SBA-15 and the original siliceous SBA-15 suggests an uniform mesoporous structure was mostly retained after cobalt grafting. The capillary condensation step of the isotherm occurred at a lower relative pressure for Co-SBA-15 as compared to the pure silica SBA-15, indicating a decrease of the mean pore diameter after cobalt grafting. The pore size of pure silica SBA-15 was 7 nm, obtained from N_2 physisorption using the BJH method (Figure 4b), while the pore size of Co-SBA-15 was 6.7 nm (Figure 4d). The decrease of the pore diameter after cobalt grafting is mostly the result from the reconstruction due to dehydroxylation rather than additional layer of cobalt formed on the inside of the silica wall. This is evident in Table 1, where it is shown that the pore contraction of SBA-15 following toluene reflux and calcination is the same as observed in the actual Co grafting process. Increasing the cobalt loading from 5.7 to 10.4 wt % does not result in additional pore diameter decrease. One of the reasons is the actual cobalt loading does not increase by a factor of 4 as the initial cobalt loading increased from 10 to 40 wt %. Another important factor is the relatively small amount of grafted cobalt only results in partial surface coverage because of the high surface area of the SBA-15 structure.

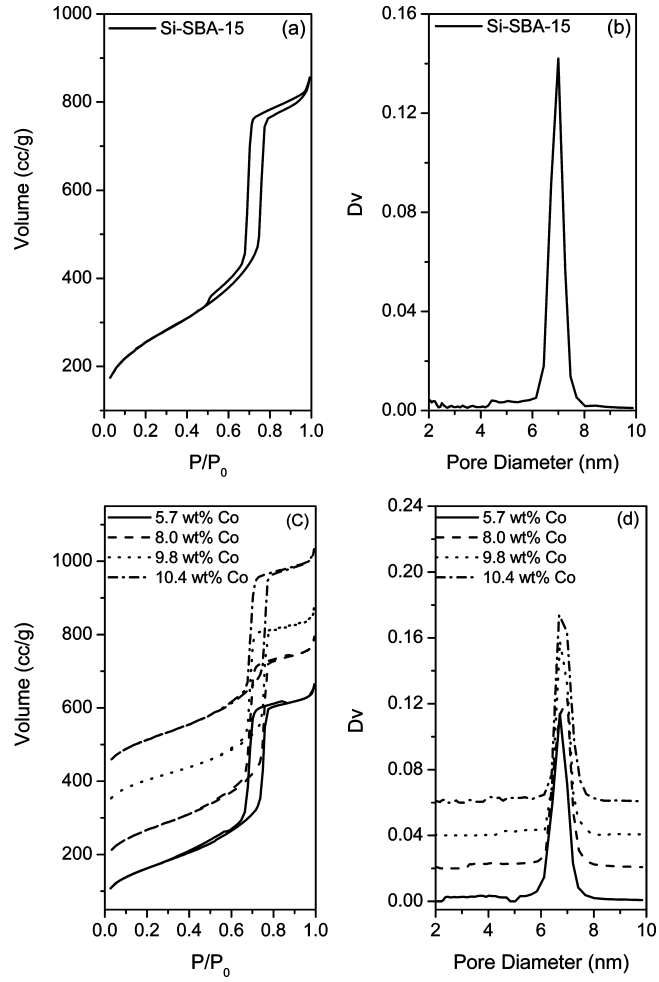

Figure 4. N_2 physisorption of cobalt-grafted SBA-15 synthesized from Co(II) acetylacetonate with different loading (a) isotherm of siliceous SBA-15, (b) pore size distribution of siliceous SBA-15, (c) isotherm of Co-SBA-15 with different initial cobalt loadings, the lines are stacked with displacement of 100 cc/g, (d) pore size distribution of Co-SBA-15 with different initial cobalt loadings, the lines are stacked with displacement of 0.02 differential volume (cc/g).

The physical properties of silica SBA-15 and Co-SBA-15 obtained from N_2 physisorption are given in Table 1. The BET surface area and pore volume for the silica SBA-15 are typical for siliceous SBA-15 synthesized under similar conditions. Both the BET surface area and total pore volume dropped after cobalt grafting. This may be caused by a partial blockage of the SBA-15 pores by cobalt particles and/or a partial collapse of the mesoporous structure during the procedure of grafting and

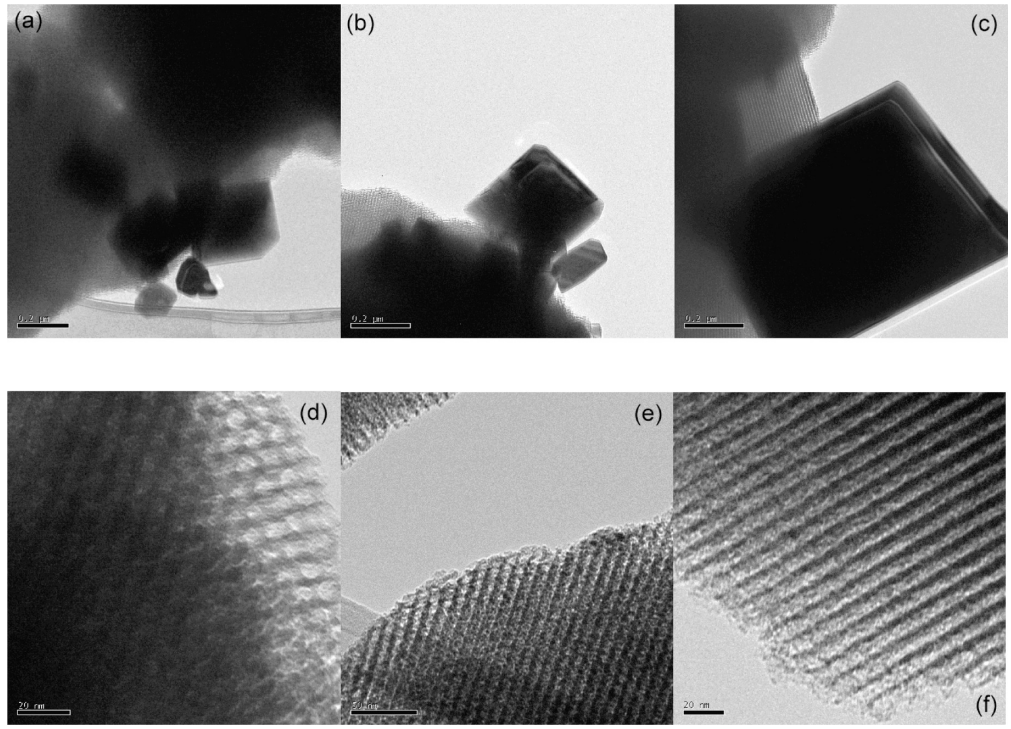

Figure 5. TEM images of Co-SBA-15 (a−c), synthesized from $CoCl_2$ (5 wt % initially), (d−f) synthesized by Co(II) acetylacetonate (5.7 wt %) (scale bar in a−c is 0.2 μm, d is 20 nm, e is 50 nm, and f is 20 nm).

recalcination or from the condensation of silanol groups on the surface. In a blank test, pure siliceous SBA-15 was refluxed in toluene for 6 h under the same conditions as for grafting cobalt. The sample was then dried in air and separated into two. In Table 1, Si-SBA-15r denotes the sample after refluxing, but without calcination. Si-SBA-15rc refers to the siliceous SBA-15 after refluxing and recalcination. Both the surface area and pore volume of the siliceous SBA-15 contracted after the refluxing, but there is no difference between air drying and calcination, which indicates the structure of SBA-15 contracted and perhaps was partially destroyed during the refluxing in toluene. However, there appears to be a small incremental decrease in surface area in the actual grafting of Co relative to that observed in SBA-15 following toluene refluxing and calcination without added Co. An improvement of this grafting method may be achieved by optimizing the refluxing time.

3.1.3. Transmission Electron Microscopy (TEM). Figure 5 shows the TEM images taken from different orientations of cobalt-grafted SBA-15 samples. All the TEM images clearly reveal the highly ordered hexagonal arrays of one-dimensional mesopores, typically representing the SBA-15 support materials, which is additional evidence that the ordered SBA-15 framework was retained after the grafting and calcination process. The difference of Co-SBA-15 synthesized by using different cobalt precursors is more obviously observed under TEM. As discussed in the XRD analysis, Co-SBA-15 synthesized from $CoCl_2$ formed large crystals of Co_3O_4 indicated in the high range of 2θ XRD patterns. Low-magnification (μm) TEM pictures proved the existence of such large crystal particles. Figure 5a−c shows the TEM images of Co-SBA-15 synthesized with $CoCl_2$ (5 wt %) taken from different parts of the samples. The large Co_3O_4 crystals were observed clearly and can be found everywhere in the samples. The size ranges from 50 nm up to hundreds of nanometers. However, TEM images taken from Co-SBA-15 synthesized from Co(II) acetylacetonate (Figure 5d−f) do not show the existence of Co_3O_4 crystals, even on a tens-of-nanometers scale which indicates that there is no bulk Co_3O_4 formed on the SBA-15 surface after calcination. All the cobalt ions are believed to be dispersed evenly on the surface of SBA-15 after the grafting and calcination treatment using Co(II) acetylacetonate precursor, and only the ordered pore structure of SBA-15 is seen in Figure 5d−f.

3.1.4. Temperature-Programmed Reduction (TPR). Hydrogen TPR is a very useful characterization technique for transition metal catalysts. By means of TPR, not only the reducibility and stability of the metal supported catalysts can be revealed but also some surface chemical information, i.e., metal species, metal distribution and quantitatively, the loading of different metal surface compounds, can be easily determined. For example, in this study, TPR was not only used to find the reduction temperature of different cobalt oxide species but also to calculate the actual cobalt loading by calibrating the reduction peak area with a standard sample, which has a known cobalt loading confirmed by chemical analysis. The temperature reduction experiment was carried out in 5% H_2/Ar from 298 to 1123 K at 5 K/min and held at 1123 K for 1 h for all the Co grafted SBA-15 samples prepared using different cobalt sources and different initial loadings, as shown in Figures 6 and 7. Figure 6 shows the TPR patterns of Co-grafted SBA-15 synthesized from $CoCl_2$. There is only one reduction peak at around 623 K, which is in the range for Co_3O_4 oxide reduction. With an increase of the initial cobalt loading, the height and the width of the reduction peaks increased. A systematic increase of the maximum reduction rate with initial cobalt content was observed. The shift of the reduction temperature to a higher range can be explained by the formation of Co_3O_4 particles. With the increase of initial $CoCl_2$ loading, there are more and larger surface crystal cobalt oxides formed. This information is also confirmed by the results of XRD, see Figure 2b, and TEM pictures, see Figure 5a−c.

Figure 7 shows the reduction patterns of the Co-grafted SBA-15 synthesized from cobalt(II) acetylacetonate with different initial loadings. Compared with the Co-SBA-15 made from $CoCl_2$, there is a significant difference in the reduction tem-

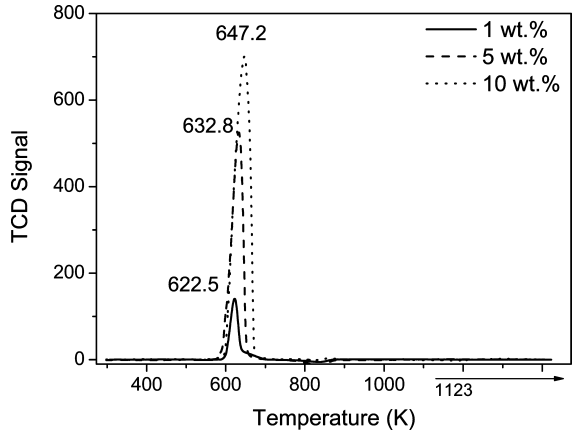

Figure 6. TPR patterns of Co-SBA-15 synthesized from $CoCl_2$ with different loadings.

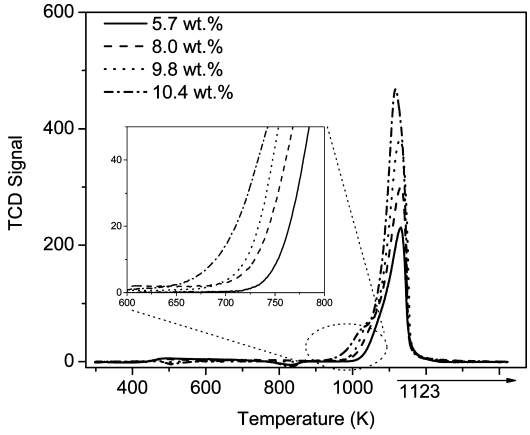

Figure 7. TPR patterns of Co-SBA-15 synthesized from Co(II) acetylacetonate with different loadings.

perature. The maximum reduction rate temperature occurred at much higher temperature, (around 1123 K). With an increase of cobalt loading, the peak area increased. However, the rate of increase in peak area was not proportional to the initial synthesis solution loading, which indicates that actual cobalt loading approached saturation at around 10 wt %. By comparing the reduction peak area with the standard sample (1 wt % Co-MCM-41), the actual cobalt loading was determined and is listed in Table 1. It should be noted that for those samples where a portion of Co remains as an oxide and contains Co_2O_3 (Co^{3+} instead of the presumed Co^{2+}) the wt % loading from TPR is not quantitative. However, for the grafted Co-SBA-15 synthesized from cobalt(II) acetylacetonate (results in Table 1), XAS indicates that Co is in the +2 oxidation state and we have previously demonstrated that TPR gives quantitative Co loading in agreement with both chemical analysis and XAS edge jump measurements when Co^{2+} is substituted in a Si cation tetrahedral site, see ref 34.

The maximum reduction rate temperature shifted a little to lower temperature with the increase of initial cobalt loading. The lowering of the reduction temperature is the result of catalytic reduction of Co^{2+} cation by Co metal and/or H_2 spill over from cobalt metal particles. The greater the cobalt loading, the more catalytic reduction/H_2 spill over occurs. Note that TPR of the $CoCl_2$ prepared Co-SBA-15 shifts to higher temperature with increased loading. That is, hydrogen spillover does not affect the rate of TPR of large (bulk) Co_3O_4 reduction which is presumably rate limited by diffusion through the large crystals.

Such high reduction temperature indicates that cobalt ions were bonded to the surface of SBA-15 in a very stable structure.

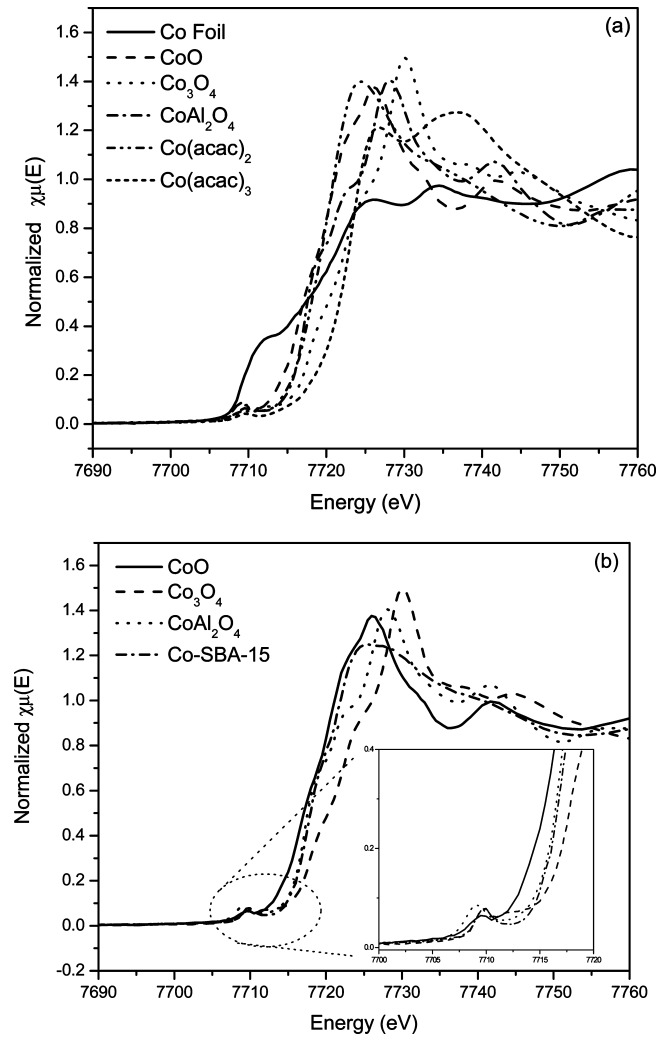

Figure 8. (a) XANES of Co foil and different cobalt references (b) comparison of XANES of Co-SBA-15 (5.7 wt %) with CoO, Co_3O_4, and $CoAl_2O_4$.

From the study of another cobalt mesoporous catalyst, Co-MCM-41, it is known that those cobalt ions were substituted for silicon in the tetrahedral surroundings bonded with oxygen. Those cobalt ions in the Co-MCM-41 have a reduction temperature of about 1073 K. These newly synthesized Co-SBA-15 samples have even higher reduction temperature than Co-MCM-41, suggesting that the cobalt ions in the Co-SBA-15 must have a similar or even more stable structure than those in Co-MCM-41. The X-ray absorption analysis discussed below demonstrates the local environment of cobalt ions is a distorted tetrahedral structure.

3.1.5. X-ray Absorption Spectroscopy Near-Edge Structure (XANES). The first-row transition metal elements have well-defined site symmetry spectra in the XANES. Figure 8 shows the normalized (to the Co edge jump, i.e., per Co atom/cation) Co K-edge XANES spectra of dehydrated Co-SBA-15 synthesized from $Co(C_5H_7O_2)_2$ compared with different cobalt reference samples. All the samples were calibrated with the cobalt foil standard edge energy at the first inflection point (K-edge) in the foil calibration spectrum (7709.0 eV), which measures the threshold of photo ejection of the 1s electron in cobalt atom or ions.

The references in Figure 8a are of three kinds: Co metal, Co oxides with both Co^{2+} and Co^{3+} ions, and Co acetylacetonate complexes with both Co^{2+} and Co^{3+} ions. Comparing the latter,

TABLE 2: XANES Data of Co-SBA-15 Comparing with Different Cobalt Reference Compounds

sample ID	pre-edge peak (eV)	main-edge peak (eV)	$E_{\text{main-edge}} - E_{\text{pre-edge}}$ (eV)
Co-SBA-15	7708.5	7717.5	9.0
$CoAl_2O_4$	7708.5	7717.0	9.0
CoO	7708.5	7720.0	11.5
Co_3O_4	7708.5 and 7711.0	7727.5	19 and 16.5

one can immediately see the effect of the change of oxidation state in the shift in both the threshold and inflection point of the edge (a shift of the order of 3 V) but the white line does not lend itself to any simple interpretation, showing essentially single- and double-peaked white lines for the Co^{2+} and Co^{3+}, respectively. For this reason, we will focus on the pre-edge intensity and edge position of the oxide references that are compared to dehydrated Co-SBA-15 in Figure 8b. Clearly, Co-SBA-15 has an edge position that is consistent with Co^{2+} aligning with CoO and $CoAl_2O_3$ and not with Co_3O_4 that contains both oxidation states. Site symmetry is reflected in the intensity of the pre-edge peak being lowest for the highest symmetry (CoO, octahedral) and highest for the lowest symmetry ($CoAl_2O_3$, tetrahedral). Both Co-SBA-15 and Co_3O_4 fall in between, but coupled with the Co^{2+} oxidation state, we surmise that it is likely to be a distorted tetrahedral environment, and this will be confirmed below by EXAFS coordination number.

The dehydrated Co-SBA-15 sample was treated thermally from room temperature to 573 K and kept at 573 K for 30 min under He to remove any adsorbed H_2O. The adsorbed H_2O on cobalt sites will contribute to the Co−O coordination number in the further EXAFS fitting and will show higher number of surrounding O of each cobalt caion. The XANES results of Co-SBA-15 and different cobalt reference samples are summarized in Table 2. The distance between the pre-edge peak and the main edge can be used to measure the oxidation state of cobalt ions. In the tetrahedral Co^{2+} compound, like $CoAl_2O_4$, this value is about 9.0 eV. The $E_{\text{main-edge}} - E_{\text{pre-edge}}$ is 11.5 eV for the octahedral Co^{2+} (CoO). With the mixing of Co^{3+} with Co^{2+}, the main-edge is shifted to higher energy. It is shifted from 7717.0 or 7720.0 eV ($CoAl_2O_4$ or CoO) to 7727.5 eV (Co_3O_4). Co-SBA-15 has a similar main-edge, pre-edge and $E_{\text{main-edge}} - E_{\text{pre-edge}}$ to that of tetrahedral Co^{2+} in $CoAl_2O_4$, which is 7708.5, 7717.0, and 9.0 eV. This suggests that Co^{2+} ions in the Co-SBA-15 have a coordination environment close to the tetrahedral structure.

While the precursor to the catalyst for synthesis to SWNT contains only oxidized Co, as discussed above, it is the Co metal particles that catalyze the disproportionation of CO and growth of SWNT. In the process used in our laboratory, we prereduce the Co-SBA-15 in hydrogen at a temperature lower than the reaction temperature before exposure to reactant CO at reaction temperature.[1,2] This results in incomplete reduction but the formation of very small Co particles which we hypothesize are anchored to unreduced Co cations.[13] The highest prereduction used in this work was 973 K. The XANES of the in situ TPR are shown in Figure 9 and compared to the reference XANES of Co foil. Here the white line intensity clearly shows that not all of the Co has been reduced to metal before reaction.

3.1.6. Extended X-ray Absorption Fine Structure (EXAFS). EXAFS can provide quantitative information about the atomic structure and ligand environment. Figure 10 shows the *R* space fitting of Co-SBA-15 sample using the first shell Co−O path. The bond length of Co−O can be calculated from the fitting to

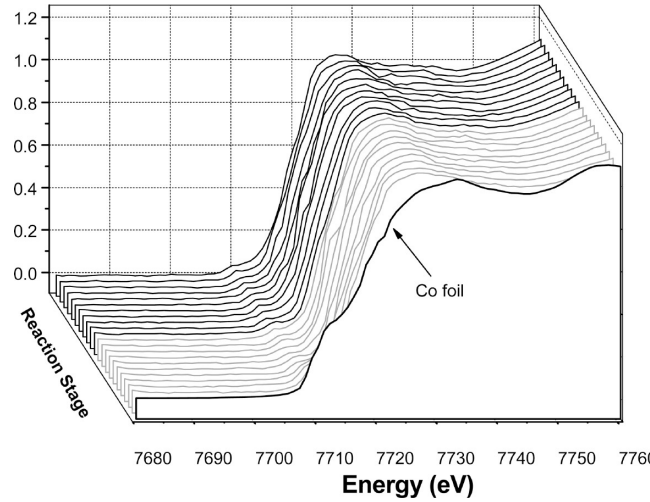

Figure 9. XANES spectra of in situ reduction of 5.7 wt % Co-SBA-15 under H_2 (black lines, ramping from room temperature to 973 K; gray lines, kept at 973 K for 30 min).

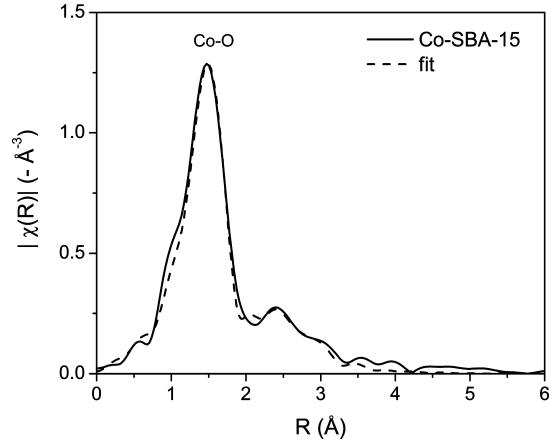

Figure 10. EXAFS *R* space fitting of Co-SBA-15 (5.7 wt %) catalyst.

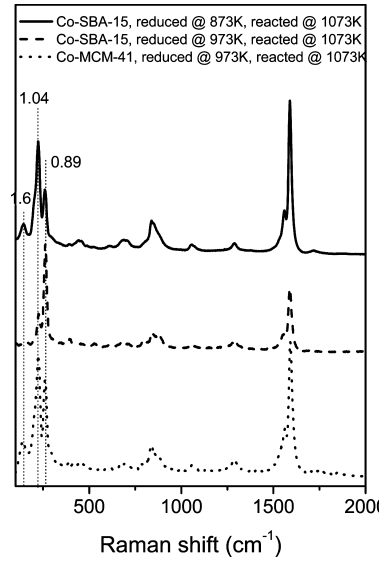

Figure 11. Comparison of Raman spectra of carbon SWNT synthesized by Co-SBA-15 (5.7 wt %) and Co-MCM-41 catalysts.

be 1.972 ± 0.012. The coordination number for Co−O is 4.73 ± 0.52, which is consistent (within uncertainty) with the hypothesis that cobalt ions are fixed in a distorted tetrahedral

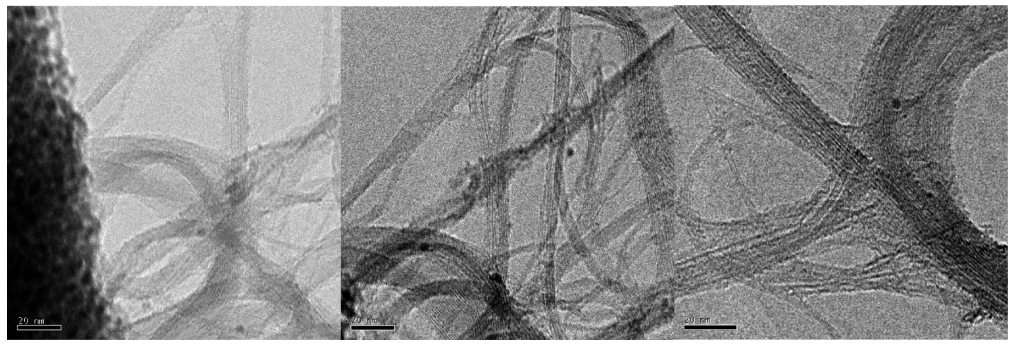

Figure 12. TEM images of carbon SWNT synthesized by Co-SBA-15 (scale bar is 20 nm in all the images).

surroundings. Such stable local environments for cobalt ions explain the high reduction stability.

3.2. Catalytic Performance of Co-SBA-15 for Carbon SWNT Synthesis. The catalytic activities of Co-SBA-15 were tested for the desired reaction: the synthesis of carbon SWNT. The reaction conditions are the same as reported for carbon SWNT synthesis using the Co-MCM-41 (C16 alkyl template) catalyst.[1,2] The catalysts were first prereduced under H_2 then reacted with CO at 1073 K. Two different prereduction temperatures were tested—873 and 973 K. The color of the catalysts changed to black visually after the reaction, which indicates the formation of some carbon species. From the Raman spectra and TEM micrographs, the existence of carbon SWNT was confirmed. Figure 11 shows the comparison of Raman spectra of carbon SWNT synthesized from Co-SBA-15 and Co-MCM-41 catalysts. The Raman spectra of the two different cobalt mesoporous catalysts show a significant G band at around 1600 cm^{-1}, which is characteristic of ordered carbon species. The relatively negligible D band at around 1300 cm^{-1} indicates that most of the carbon species are in the form of carbon SWNT with only very a small amount of amorphous carbon impurity. The radial breathing mode (RBM) below 350 cm^{-1} can be used to estimate the diameter of carbon nanotubes. Three different diameter carbon nanotubes are observed, 0.89, 1.04, and 1.6 nm. For Co-SBA-15 catalyst, at the low prereduction temperature (873 K), a 1.04 nm diameter tube is the major species, which is similar to the synthesis using Co-MCM-41 (C16 alkyl template prereduced at 973 K) catalyst. However, when the prereduction temperature is increased to 973 K, the smaller tube (0.89 nm) becomes the majority species. The ratio of 0.89 nm peak to 1.04 nm peak changed from 1:5 to 5:1 on Co-SBA-15 when the prereduction temperature is increase from 873 to 973 K. That is, Co-SBA-15 favors smaller diameter SWNT relative to C16 Co-MCM-41 compared at the same prereduction and reaction temperature. This is similar to the C10 Co-MCM-41, which is another incorporated Co-MCM-41 catalyst with a smaller diameter framework (1.9 nm).[34] From the result of TPR, C10 Co-MCM-41 also exhibits higher reduction stability compared with C16 Co-MCM-41 and narrower peak. This indicates that at the high-temperature reduction and reaction conditions, both C10 Co-MCM-41 and Co-SBA-15 catalysts can create more stable small reduced Co metal particles than C16 Co-MCM-41. Note that it is the higher reduction stability that C10 Co-MCM-41 and Co-SBA-15 have in common with regard to synthesis, of smaller diameter SWNT, because C10 Co-MCM-41 has smaller pores and Co-SBA-15 larger pores than C16 C0-MCM-41. Such high reduction stability will result in higher selectivity to smaller diameter SWNT as a result of anchoring of smaller Co metal particles. Thus, increasing the prereduction temperature of Co-SBA-15 increases the selectivity to smaller size carbon SWNT dramatically. This is an interesting result because the size of synthesized carbon SWNT can be controlled by varying the prereduction temperature and the reaction temperature.[34]

The yield of the carbon SWNT synthesized from Co-SBA-15 based on the total weight of catalyst were measured with TGA. It increased from 3.2% to 5.7% when the prereduction temperature was increased from 873 to 973 K. This is because within the certain temperature range, the higher prereduction temperature means more reduced cobalt metal particles, which correlates with the yield of carbon SWNT. Compared with the Co-MCM-41 catalyst, which has about 3.0 wt % yield prereduced at 973 K and reacted at same temperature,[1,2] the yield doubles for the Co-SBA-15 (6 wt % cobalt loading) because of its high-capacity Co loadings. That is, in the comparison being made to 3 wt % Co-MCM-41 with 5.7 wt % Co-SBA-15, the increased yield is simply proportional to the increased loading of Co and, assuming comparable Co metal particle size as indicated by the XAS, all the yield increase can be accounted for by loading suggesting that the larger pores of Co-SBA-15 have not resulted in a higher rate of reaction.

Figure 12 shows TEM micrographs of carbon SWNT synthesized with Co-SBA-15. Bundled small-diameter SWNTs can be clearly viewed everywhere coming out of the SBA-15 framework. The small black dots are the reduced cobalt particles. The diameter of such small tubes can be estimated to be around 1 nm from TEM images, which is consistent with the calculation from RBM in the Raman spectra.

4. Conclusion

Highly dispersed cobalt SBA-15 was successfully synthesized by a postsynthesis method using $Co(C_5H_7O_2)_2$ as the cobalt source. By utilizing different characterization techniques, high dispersion of isolated cobalt sites was confirmed. The physical structure of SBA-15 was mostly retained after cobalt grafting. One of the most interesting chemical properties of Co-SBA-15 was its high-temperature reducibility; it exhibits a maximum reduction rate at 1123 K in TPR. Such high-reduction stability results from all the cobalt ions being isolated and dispersed in a stable environment. X-ray absorption analysis further demonstrated the isolated cobalt sites, a Co^{2+} oxidation state and a Co−O coordination number of 4.73 ± 0.52, which is consistent with a distorted tetrahedral environment.

The high reduction stability makes Co-SBA-15 a favorable catalyst for high-temperature catalytic reactions, e.g., synthesis of carbon SWNT. Raman spectroscopy and TEM images showed very good quality of carbon SWNTs synthesized with Co-SBA-15. Compared with Co-MCM-41 (C16 template) at the same prereduction and reaction conditions, Co-SBA-15 has a higher yield of carbon SWNT and favors a smaller average diameter product. Co-SBA-15 has a similar high reduction

stability to Co-MCM-41 (C10 template) relative to Co-MCM-41 (C16 template). Both Co-MCM-41 (C10 template) and Co-SBA-15 are more stable against reduction in TPR and have a narrower reduction peak. The smaller SWNT average diameter can be associated with smaller, stable Co particles on which the SWNTs grow.

Acknowledgment. The authors are grateful to Department of Energy, Office of Basic Energy Services, Grant No. DOE FG02-01ER15183 for funding this project and thank the National Synchrotron Light Source at Brookhaven National Laboratory for beam time.

References and Notes

(1) Chen, Y.; Ciuparu, D.; Lim, S.; Yang, Y.; Haller, G. L.; Pfefferle, L. *J. Catal.* **2004**, *226*, 351.
(2) Chen, Y.; Ciuparu, D.; Lim, S.; Yang, Y.; Haller, G. L.; Pfefferle, L. *J. Catal.* **2004**, *225*, 453.
(3) Ciuparu, D.; Chen, Y.; Lim, S.; Haller, G. L.; Pfefferle, L. *J. Phys. Chem. B* **2004**, *108*, 10196.
(4) Ciuparu, D.; Chen, Y.; Lim, S.; Haller, G. L.; Pfefferle, L. *J. Phys. Chem. B* **2004**, *108*, 503.
(5) Ciuparu, D.; Chen, Y.; Lim, S.; Yang, Y.; Haller, G. L.; Pfefferle, L. *J. Phys. Chem. B* **2004**, *108*, 15565.
(6) Ciuparu, D.; Chen, Y.; Lim, S.; Yang, Y.; Haller, G. L.; Pfefferle, L. *Polym. Prepr. (Am. Chem. Soc., Div. Polym. Chem.)* **2005**, *46*, 206.
(7) Li, Y. M.; Kim, W.; Zhang, Y. G.; Rolandi, M.; Wang, D. W.; Dai, H. J. *J. Phys. Chem. B* **2001**, *105*, 11424.
(8) Kukovitsky, E. F.; L'vov, S. G.; Sainov, N. A.; Shustov, V. A.; Chernozatonskii, L. A. *Chem. Phys. Lett.* **2002**, *355*, 497.
(9) Dal, H. J.; Rinzler, A. G.; Nikolaev, P.; Thess, A.; Colbert, D. T.; Smalley, R. E. *Chem. Phys. Lett.* **1996**, *260*, 471.
(10) Bolshakov, A. P.; Uglov, S. A.; Saveliev, A. V.; Konov, V. I.; Gorbunov, A. A.; Pompe, W.; Graff, A. *Diamond Relat. Mater.* **2002**, *11*, 927.
(11) Lim, S.; Ciuparu, D.; Pak, C.; Dobek, F.; Chen, Y.; Harding, D.; Pfefferle, L.; Haller, G. *J. Phys. Chem. B* **2003**, *107*, 11048.
(12) Lim, S.; Ciuparu, D.; Yang, Y. H.; Du, G. A.; Pfefferle, L. D.; Haller, G. L. *Microporous Mesoporous Mater.* **2007**, *101*, 200.
(13) Lim, S. Y.; Wang, C.; Yang, Y. H.; Ciuparu, D.; Pfefferle, L.; Haller, G. L. *Catal. Today* **2007**, *123*, 122.
(14) Zhao, D. Y.; Huo, Q. S.; Feng, J. L.; Chmelka, B. F.; Stucky, G. D. *J. Am. Chem. Soc.* **1998**, *120*, 6024.
(15) Zhao, D. Y.; Feng, J. L.; Huo, Q. S.; Melosh, N.; Fredrickson, G. H.; Chmelka, B. F.; Stucky, G. D. *Science* **1998**, *279*, 548.
(16) Wang, Y.; Noguchi, M.; Takahashi, Y.; Ohtsuka, Y. *Catal. Today* **2001**, *68*, 3.
(17) Martinez, A.; Lopez, C.; Marquez, F.; Diaz, I. *J. Catal.* **2003**, *220*, 486.
(18) White, M. G. *Catal. Today* **1993**, *18*, 73.
(19) VanderVoort, P.; Possemiers, K.; Vansant, E. F. *J. Chem. Soc., Faraday Trans.* **1996**, *92*, 843.
(20) VanDerVoort, P.; Babitch, I. V.; Grobet, P. J.; Verberckmoes, A. A.; Vansant, E. F. *J. Chem. Soc., Faraday Trans.* **1996**, *92*, 3635.
(21) Van der Voort, P.; White, M. G.; Vansant, E. F. *Langmuir* **1998**, *14*, 106.
(22) Van Der Voort, P.; van Welzenis, R.; de Ridder, M.; Brongersma, H. H.; Baltes, M.; Mathieu, M.; de Ven, P. C.; Vansant, E. F. *Langmuir* **2002**, *18*, 4420.
(23) Sekine, R.; Kawai, M.; Asakura, K.; Hikita, T.; Kudo, M. *Surf. Sci.* **1992**, *278*, 175.
(24) Kenvin, J. C.; White, M. G.; Mitchell, M. B. *Langmuir* **1991**, *7*, 1198.
(25) Haukka, S.; Lakomaa, E. L.; Suntola, T. *Appl. Surf. Sci.* **1994**, *75*, 220.
(26) Collart, O.; Van der Voort, P.; Vansant, E. F.; Gustin, E.; Bouwen, A.; Schoemaker, D.; Rao, R. R.; Weckhuysen, B. M.; Schoonheydt, R. A. *Phys. Chem. Chem. Phys.* **1999**, *1*, 4099.
(27) Baltes, M.; Collart, O.; Van der Voort, P.; Vansant, E. F. *Langmuir* **1999**, *15*, 5841.
(28) Segura, Y.; Cool, P.; Van Der Voort, P.; Mees, F.; Meynen, V.; Vansant, E. F. *J. Phys. Chem. B* **2004**, *108*, 3794.
(29) Herrera, J. E.; Kwak, J. H.; Hu, J. Z.; Wang, Y.; Peden, C. H. F.; Macht, J.; Iglesia, E. *J. Catal.* **2006**, *239*, 200.
(30) Brunauer, S.; Emmett, P. H.; Teller, E. *J. Am. Chem. Soc.* **1938**, *60*, 309.
(31) Barrett, E. P.; Joyner, L. G.; Halenda, P. P. *J. Am. Chem. Soc.* **1951**, *73*, 373.
(32) Stern, E. A.; Newville, M.; Ravel, B.; Yacoby, Y.; Haskel, D. *Phys. B: Condens. Matter* **1995**, *209*, 117.
(33) Ankudinov, A. L.; Ravel, B.; Rehr, J. J.; Conradson, S. D. *Phys. Rev. B* **1998**, *58*, 7565.
(34) Lim, S.; Li, N.; Fang, F.; Pinault, M.; Zoican, C.; Wang, C.; Fadel, T.; Pfefferle, L. D.; Haller, G. L. *J. Phys. Chem. C* **2008**, *112*, 12442.

JP901823V